Article

Satellite-Derived Spatiotemporal Variations in Evapotranspiration over Northeast China during 1982–2010

Lilin Zhang [1,2]**, Yunjun Yao** [1,2,*]**, Zhiqiang Wang** [3]**, Kun Jia** [1,2] iD **, Xiaotong Zhang** [1,2]**, Yuhu Zhang** [4]**, Xuanyu Wang** [1,2]**, Jia Xu** [1,2] **and Xiaowei Chen** [1,2]

[1]   State Key Laboratory of Remote Sensing Science, Faculty of Geographical Science, Beijing Normal University, Beijing 100875, China; 201521170059@mail.bnu.edu.cn (L.Z.); jiakun@bnu.edu.cn (K.J.); xtngzhang@bnu.edu.cn (X.Z.); skywalkerwxy@163.com (X.W.); diamond1201@sina.cn (J.X.); 18368091857@163.com (X.C.)

[2]   Beijing Engineering Research Center for Global Land Remote Sensing Products, Institute of Remote Sensing Science and Engineering, Faculty of Geographical Science, Beijing Normal University, Beijing 100875, China

[3]   National Disaster Reduction Center/Satellite Application Center for Disaster Reduction of the Ministry of Civil Affairs, Beijing 100124, China; wzqbnu@163.com

[4]   College of Resource Environment and Tourism, Capital Normal University, Beijing 100048, China; zhang_yuhu@163.com

*   Correspondence: boyyunjun@163.com; Tel.: +86-10-5880-3002

Abstract: Evapotranspiration (ET) is a critical process for the climate system and water cycles. However, the spatiotemporal variations in terrestrial ET over Northeast China over the past three decades calculated from sparse meteorological point-based data remain large uncertain. In this paper, a recently proposed modified satellite-based Priestley–Taylor (MS–PT) algorithm was applied to estimate ET of Northeast China during 1982–2010. Validation results show that the square of the correlation coefficients (R^2) for the six flux tower sites varies from 0.55 to 0.88 ($p < 0.01$), and the mean root mean square error (RMSE) is 0.92 mm/d. The ET estimated by MS–PT has an annual mean of 441.14 ± 18 mm/year in Northeast China, with a decreasing trend from southeast coast to northwest inland. The ET also shows in both annual and seasonal linear trends over Northeast China during 1982–2010, although this trend seems to have ceased after 1998, which increased on average by 12.3 mm per decade pre-1998 ($p < 0.1$) and decreased with large interannual fluctuations post-1998. Importantly, our analysis on ET trends highlights a large difference from previous studies that the change of potential evapotranspiration (PET) plays a key role for the change of ET over Northeast China. Only in the western part of Northeast China does precipitation appear to be a major controlling influence on ET.

Keywords: evapotranspiration; Northeast China; MS–PT algorithm; spatial-temporal variations; controlling factors; potential evapotranspiration

1. Introduction

Over the past three decades, global warming has influenced the climate condition and the hydrological cycle of Northeast China [1,2]. Especially for evapotranspiration (ET), it is an important process in an ecosystem water budget, energy balance, and carbon cycles, and strongly affects surface dry conditions and climate change [3–5]. Numerous studies have reported that significant changes in ET are influencing ecosystem processes, surface drought conditions, and the consequent local climate feedback over Northeast China [6–11]. Based on the meteorological measurements, the annual reference ET (ET_0) of Northeast China has increased at a rate of 3.89 mm/decade during 1961–2007,

with large interannual fluctuations [12]. However, due to a lack of direct measurements, there are still large biases in estimating the actual ET for the detection of variations in water budget and surface drought in Northeast China. Therefore, it is urgent to improve ET estimation and evaluate the long-term variation of ET for understanding the hydrologic changes and solving problems in water resource management.

Based on the large ground-measurements, several traditional approaches have been widely used to estimate ET in Northeast China. Among them, eddy covariance data can be considered to be reliable for quantifying ET at the local scale [13,14]. However, since their measurements are of short duration and sparse spatial coverage, they cannot provide long-term regional estimates of ET [15]. Similarly, the application of traditional ET estimation models, whose parameters derived mostly from field observations, is greatly restricted in Northeast China [16]. For example, Gao et al. [7] used the water balance methodology to estimate monthly ET for 686 stations over China and found the actual ET tends to decrease in most areas of Northeast China during 1960–2002. Nevertheless, due to the problem of scale conversion, such ET methods require a very large amount of ground-observation data and can only be accurate at the local scale [3].

Currently, remote sensing has provided real-time and dynamic information for terrestrial energy systems, facilitating effective regional ET estimation [17,18]. Based on satellite-based observations, several approaches have been used to estimate the spatial and temporal variation in ET over Northeast China. For instance, Tian et al. [19] combined water balance components and surface energy balance components by Noah land surface model and found decreasing changes in ET over Northeast China during 1986–2008. Based on global Moderate Resolution Imaging Spectroradiometer (MODIS) ET products, Tian et al. [20] reported that ET shows a positive trend in the Northeast Plain during 2001–2010 and attributed this trend to the change of vegetation condition. Yang et al. [21] using the GLEAM (global land-surface evaporation: the Amsterdam methodology) model, documented a negative trend in the western part of Northeastern China during the 1981 to 2010 period and pointed out that the annual trend shows a remarkable correlation with the trend in summer. Although these studies have focused on the detection of variation in ET over Northeast China, due to the difference in model structures and dominant variables, the interannual variability of ET vary significantly between models [22]. Large uncertainties in the spatial-temporal variation of ET over long time periods still remain in Northeast China. A recently modified satellite-based Priestley–Taylor (MS–PT) algorithm proposed by Yao et al. [23] has been used to estimate ET in mainland China. According to validation for 16 EC flux tower sites throughout China, the average RMSE between measured and predicted site-averaged daily ET was approximately 5 W/m^2 lower (99% confidence) for the MS–PT compared to the Priestley–Taylor-based ET (PT–JPL) algorithm. It is physically based, requiring no subjective parameter calibrations as employed by many other traditional methods, which exactly solved the problem of insufficient input data. Importantly, this method is also satisfactory in detecting the interannual variability in China [24]. However, there is a lack of similar studies that simulate regional terrestrial ET over Northeast China by using the MS–PT algorithm and satellite datasets. As a result, little is accurately understood regarding spatiotemporal characterization of the response of regional terrestrial ET to climate change for long periods.

In this study, we used the MS–PT algorithm driven by remote sensing data and meteorological reanalysis data to estimate ET in Northeast China. We had two major objectives. First, we evaluated the performance of the MS–PT algorithm using ground-measured flux data collected from six flux towers in Northeast China. Second, we analyzed the spatiotemporal variation in ET from 1982 to 2010 and detected the issue of what factors contribute to the variability and trends of ET in Northeast China.

2. Materials and Methods

2.1. Study Area

Northeast China (38°42′–53°55′N, 115°32′–135°09′E) is located in a transition region between the subarctic region and temperate region [25]. The total area is approximately 1.24×10^6 km^2, covering four provinces, including Heilongjiang, Jilin, and Liaoning, and some areas of the Inner Mongolia Autonomous Region: Hulun Buir, Xingan Meng, Tongliao, and Chifeng. The study area has a typical continental monsoon climate with cold, dry winters and warm, wet summers. According to a previous study, the annual precipitation of Northeast China is about 489 mm, of which 75% falls in the period of June to September [26]. The annual average temperature is about 1.9 °C–5.3 °C, and has increased at a rate of 0.34/decade during 1959–2002 [1]. Due to the suitable plant growth environment, Northeast China not only produces a large quantity of grain, but also has abundant forest reserves, which accounts for more than 1/3 of total in China [27]. The natural vegetation of Northeast China includes the forest steppe or meadow steppe, typical steppe, and desert steppe, rendering the ecological environment sensitive and fragile. A previous study illustrates that extreme precipitation and dryness events have become more and more frequent and intensified [6].

The study area can be divided into two major basins: Liaohe (LH) basin and Songjiang (SJ) basin (Figure 1). These two basins have different climatic and hydrological characteristics. For instance, the land use type of the LH basin is mainly cropland and desert land [28], which has severe water environment problems. Although the utilization rate of water resources is high, the water resources of the LH basin are still quite limited [29]. On the contrary, the land use type of the SJ basin is mainly forestland and cropland [30]. Since the annual precipitation of the SJ basin varies significantly, droughts and floods occurred frequently [31]. Separating Northeast China into these two basins will be helpful to evaluate the ET variability.
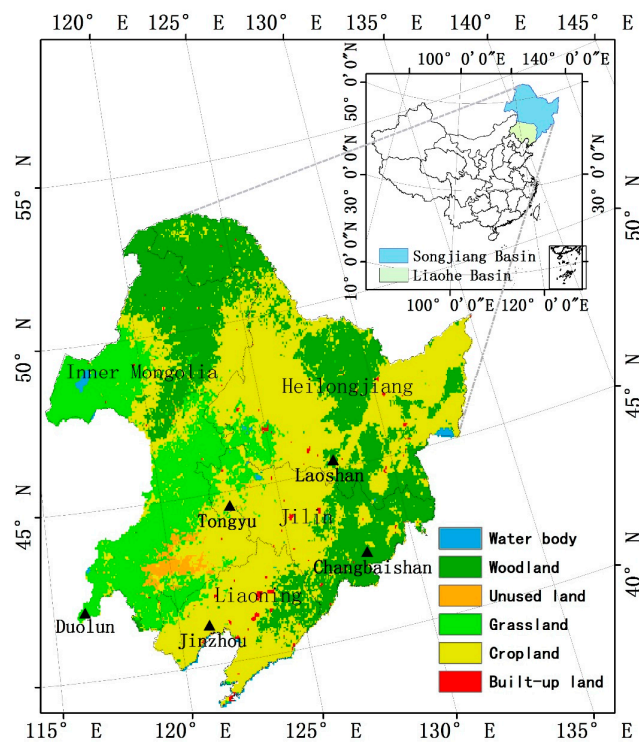
Figure 1. Map of the land cover type and the location of flux towers (Jinzhou, Duolun, Changbaishan, Tongyu, Laoshan) in Northeast China. The two main basins are also shown in inset panel: Songjiang (SJ) basin and Liaohe (LH) basin.

2.2. Data

2.2.1. Remote Sensing Data

To estimate long-term ET over Northeast China, we use the Global Inventory Modeling and Mapping Studies (GIMMS) NDVI3g data (1982–2010) generated from the Advanced Very High Resolution Radiometer (AVHRR). The GIMMS NDVI3g product contains global bimonthly NDVI at 8 km spatial resolution and can be obtained from National Oceanic and Atmospheric Administration (NOAA) [32]. In our study, the GIMMS NDVI3g data was converted to a resolution of $0.1° \times 0.1°$ using bilinear interpolation and temporally interpolated from the bimonthly averages to a daily value using linear interpolation.

To evaluate the performance of the MS–PT algorithm, the MOD16 eight-day ET product with 1 km spatial resolution is used to compare with the estimated ET. The MOD16 product is available from the National Aeronautics and Space Administration (NASA) Land Processes Distributed Active Archive Center (LP DAAC) [33]. The MOD16 product is based on the Penman–Monteith equation and uses daily meteorological reanalysis data and eight-day vegetation dynamics as inputs [34,35].

We also use the Climate Prediction Center soil moisture dataset (1982–2010) and MODIS land cover type product (MCD12C1). The soil moisture dataset provided by the NOAA [36] contains monthly averaged soil moisture at 0.5 degree and can be used to analyze the relationship with ET. The MCD12C1 data from 2001 to 2010 can be obtained online [33] and the spatial resolution of the data is 0.05 degrees.

2.2.2. Meteorological Reanalysis Data

The China Meteorological Forcing Dataset was produced by merging a variety of surface meteorological and environmental data sources, including instantaneous near surface air temperature, pressure, relative humidity, wind speed, precipitation, and surface downward shortwave radiation. To estimate the spatiotemporal variations in ET over Northeast China, we use the daily gridded meteorological reanalysis dataset as input parameters (except precipitation) to calculate ET during 1982–2010 [37]. The independent precipitation data is used to analyze the relationship with ET. This daily meteorological reanalysis dataset covers the period 1981–2010, with a resolution of 0.1 deg and 3 h. This dataset can be used for hydrological modeling, land surface modeling, land data assimilation, and other terrestrial modeling. Previous studies demonstrated that this dataset provides more accurate meteorological parameters than other reanalysis and satellite products, with less RMSE and higher correlation coefficients [38,39].

2.2.3. Ground-Based Observations

To evaluate the performance of both MS–PT algorithm on the site scale, we use the ground-observed data from six flux towers, which are distributed all around Northeast China (Figure 1). The data are provided by ChinaFLUX, LathuileFlux, and the Coordinated Enhanced Observation Network of China (CEOP) [40]. The basic information of flux observation site is shown in Table 1. All sites are based on the eddy correlation (EC) method [41,42]. Although the EC method has been widely used in the global measurement experiment, this method does not conserve energy. Therefore, in this study, we have selected the method developed by Twine et al. [43] to correct the ET from all flux towers.

Table 1. Location of the six flux towers used in this study.

Site Name	Lat, Lon	Elevation(m)	Land Cover Type	Time Period	Network
Changbaishan, Jilin	42.40°N, 128.10°E	761	Mixed forest	2002–2007	China Flux
Laoshan, Heilongjiang	45.28°N, 127.58°E	340	Larch forest	2001–2007	China Flux
Duolun1, Inner Mongolia	42.045°N, 116.671°E	1350	Cropland	2006	Lathuile-Flux
Jinzhou, Liaoning	41.18°N, 121.21°E	22.3	Cropland (maize)	2008–2009	CEOP
Duolun2, Inner Mongolia	42.047°N, 116.284°E	1350	Grassland	2006	Lathuile-Flux
Tongyu, Jilin	44.57°N, 122.88°E	184	Grassland	2008	CEOP

2.3. Methods

2.3.1. MS–PT Algorithm

The value of ET can be influenced by numerous factors, including surface moisture, stomatal conductance, air temperature (Tair), surface radiation energy [44]. Priestley and Taylor [45] combined theoretical and practical experiences and proposed a simple ET equation:

$$\text{ET} = \alpha \frac{\Delta}{\Delta + \gamma}(R_n - G) \tag{1}$$

where α is the PT coefficient and Δ is the slope of the saturated vapor pressure curve (kPa/°C). γ is the psychometric constant (kPa/°C). R_n is the surface net radiation (W/m^2). G represents the soil heat flux (W/m^2). The Priestley–Taylor algorithm solve the uncertainty of the resistances in the Penman–Monteith equation and can be accurate where aerodynamic and surface resistance is not available [44,46]. Based on the Priestley–Taylor algorithm, many revised approaches to estimate ET have been built. However, these methods require a continuum of soil moisture and vegetation status to acquire the surface conditions [46].

To minimize the need for ancillary meteorological data while maintaining a physically-realistic representation of evapotranspiration process, Yao et al. [23] modified the Priestley–Taylor [45] algorithm by using vegetation indices (VIs) and apparent thermal inertia (ATI) as the primary parameters and propose the MS–PT algorithm:

$$\text{ET} = ET_s + ET_c + ET_{ws} + ET_{ic} \tag{2}$$

The MS–PT algorithm separates the total ET into the unsaturated soil evaporation (ET_S), the canopy transpiration (ET_C), the saturated wet soil surface evaporation (ET_{ws}), and the canopy interception evaporation (ET_{ic}). Unsaturated soil evaporation can be expressed as

$$ET_s = (1 - f_{wet})f_{sm}\alpha \frac{\Delta}{\Delta + \gamma}(R_{ns} - G) \tag{3}$$

where f_{wet} is the wet surface fraction ($f_{sm}{}^4$), f_{sm} can be derived from ATI (ATI = $(1/\text{DT})^{\text{DT/DTmax}}$). DT is the diurnal air temperature range (DT$_{max}$ = 40 °C). R_{ns} is the surface net radiation to the soil ($R_{ns} = R_n(1 - f_c)$), f_c is the vegetation cover fraction ($f_c = (\text{NDVI} - \text{NDVI}_{min})/(\text{NDVI}_{max} - \text{NDVI}_{min})$). NDVI$_{min}$ and NDVI$_{max}$ are the minimum and maximum NDVI during the study period, respectively.

R_n is the surface net radiation and can be calculated using the method of Wang et al. [47]. G is the sum of the soil heat flux and can be calculated using a simple empirical R_n-based algorithm ($0.18(1 - f_c)R_n$) [24].

Canopy transpiration can be calculated using a modified linear two-source model:

$$ET_c = (1 - f_{wet})f_c f_T \alpha \frac{\Delta}{\Delta + \gamma} R_{nv} \tag{4}$$

where f_T represents plant temperature constraint ($\exp(-(T_{max} - T_{opt})/T_{opt})2)$, T_{opt} is an optimum temperature (25 °C). R_{nv} represents the surface net radiation to the vegetation ($R_{nv} = R_n f_c$).

Saturated wet soil surface evaporation can be described as

$$ET_{ws} = f_{wet}\alpha \frac{\Delta}{\Delta + \gamma}(R_{ns} - G) \tag{5}$$

Vegetation interception evaporation can be calculated from the following equation:

$$ET_{ic} = f_{wet}\alpha \frac{\Delta}{\Delta + \gamma} R_{nv} \tag{6}$$

2.3.2. Potential ET Estimation

Potential evapotranspiration (PET) is an important indicator of atmospheric evaporation demand and refers to ideal evaporation rate when soil moisture is abundant. In this study, the FAO Penman–Monteith (PM) method driven by meteorological reanalysis data and NDVI3g data was used to estimate PET of Northeast China, which was validated to all basins of China in previous studies [48,49]. The PET estimation method can be expressed as

$$\text{PET} = \frac{0.408\Delta(R_n - G) + \gamma\left(\frac{900}{T_{air}+273}\right)WS(e_s - e))}{\Delta + \gamma(1 + 0.34WS)} \tag{7}$$

where WS is the wind speed, e_s is the saturated vapor pressure, and e refers to air water vapor pressure. VPD is vapor pressure deficit and equals to $e_s - e$.

2.3.3. Statistical Analysis

The Mann–Kendall test, proposed by Mann [50] and improved by Kendall [51], is a nonparametric method for testing trends in hydrological processes and other related physical variables [52]. The null hypothesis H_0 suggests that the data are a sample of independent variables and the hypothesis H_1 states that the distribution of x_k and x_j are not identical for all $k, j \le n$ with $k \ne j$. The test statistic is given as follows:

$$S = \sum_{j=1}^{n-1} \sum_{k=j+1}^{n} \text{sgn}(x_k - x_j) \tag{8}$$

where x is the individual data values, n is the total number of data, and

$$\text{sgn}(x_k - x_j) = \begin{cases} 1 & x_k - x_j > 0 \\ 0 & x_k - x_j = 0 \\ -0 & x_k - x_j < 0 \end{cases} \tag{9}$$

The statistic *S* is nearly normally distributed, and the statistic Z is a standard normal variable:

$$Z = \begin{cases} \dfrac{s-1}{\sqrt{Var(S)}} & S > 0 \\ 0 & S = 0 \\ \dfrac{s+1}{\sqrt{Var(S)}} & S < 0 \end{cases} \tag{10}$$

$$Var(S) = \frac{1}{18}\left[n(n+1)(2n+5) - \sum_{i=1}^{n} t_i(t_i - 1)(2t_i + 5)\right] \tag{11}$$

where *i* is the number of tied groups, and t_i is the number of data values in the group. The presence of a statistically significant trend is evaluated using the Z value: positive (negative) value of Z indicates an upward (downward) trend. The null hypothesis H_0 that Z is statistically significant or not is determined by whether $-Z_{1-\alpha/2} \leq Z \leq Z_{1-\alpha/2}$, where $\pm Z_{1-\alpha/2}$ are the standard normal deviates obtained from the standard normal cumulative distribution tables, and α is the significance level for the test.

The Mann–Kendall test is also satisfactory for estimating the magnitude of the trend. The Kendall slope can be obtained by an unbiased estimator of trend magnitude:

$$\beta = \text{Median}\left(\frac{x_i - x_j}{i - j}\right) \tag{12}$$

where x_i is the annual value of ET or other meteorological elements.

3. Results

### 3.1. Evaluation of MS–PT Performance in Estimating ET

To evaluate the ability of the MS–PT algorithm to estimate ET over Northeast China, we have validated the MS–PT algorithm at daily timescales based on the EC observations. Figure 2 shows that the bias of the estimated daily ET using the MS–PT algorithm varies from 0.02 to 0.85 mm/d with a mean value of 0.33 mm/d, the root mean square error (RMSE) varies from 0.69 to 1.43 mm/d with a mean value of 0.92 mm/d, and the square of correlation coefficients (R^2) varies from 0.55 to 0.88 ($p < 0.01$) with a mean value of 0.68. Since the sites have different biomes, a comparison of the site-averaged ET demonstrates the ability of MS–PT algorithm to estimate spatial variation in ET, as shown in Figure 3. The RMSE of the comparison is 0.43 mm/d and the R^2 is 0.93. Batra et al. [53] showed that ET was estimated with an RMSE of 1.85, 1.78, and 1.97 from MODIS, NOAA16, and NOAA14 sensors, respectively. Seguin et al. [54] proposed that the majority of published remote sensing methods for estimating ET had an accuracy of ±1.5 mm/d. Kalma et al. [55] summarized most remote sensing ET models have an average RMSE just over 1.75 mm/d. Therefore, the good accuracy of the MS–PT algorithm indicates that the model has a potential to be used for analyzing ET patterns in Northeast China.

A statistical comparison of MS–PT monthly estimations and MOD16 monthly products illustrates that the MS–PT algorithm provides a more favorable agreement with the ground-measured data at most sites (except Laoshan station). The MODIS monthly ET are composed of MOD16 eight-day products. As shown in Table 2, the average monthly R^2 of MOD16 products for all sites is 0.67 and the average RMSE is 21.02 mm/month. In contrast, the ET simulations using the MS–PT algorithm has a higher R^2 (0.8) and lower RMSE (19.68 mm/month). The negative bias of both MOD16 products (−22.4 mm/month) and MS–PT model (−12.5 mm/month) may be owing to the unclosed energy balance problem in the eddy covariance datasets [42]. One should note that the R^2 of MOD16 is higher than it of MS–PT in the Laoshan station, which may be related to the quality of the observation data. To further illustrate the performance of the MS–PT algorithm to detect the interannual variability in ET, we map the monthly variations of ET over Northeast China from 2001 to 2010 (Figure 4). The flux

tower site Changbaishan was selected, where at least five years of observation are available. As shown in Figure 4, the monthly variations of ET are well captured by MS–PT-estimated ET, with a lower RMSE and a higher R^2. Thus, we can know clearly that the MS–PT algorithm improves the ET estimates at most flux towers sites and shows a better ability to detect the interannual variability in ET at different sites.

Table 2. Statistics of estimated eight-day evapotranspiration (ET) against the eddy-flux tower observations. All R^2 values are significant with a 99% confidence.

| Site Name	Bias (mm/Month)		RMSE (mm/Month)		R^2	
	MS–PT	MOD16	MS–PT	MOD16	MS–PT	MOD16
Changbaishan	−11.04	−13.14	18.68	22.13	0.94	0.92
Laoshan	−7.35	−13.54	25.39	25.5	0.76	0.79
Duolun1	−7.93	−18.37	15.71	32.24	0.91	0.63
Jinzhou	−27.78	−42.13	30.15	47.09	0.46	0.46
Duolun2	−9.52	−11.26	13.86	20.58	0.9	0.65
Tongyu	−11.38	−35.96	14.3	38.55	0.85	0.56
ALL	−12.5	−22.4	19.68	21.02	0.8	0.67
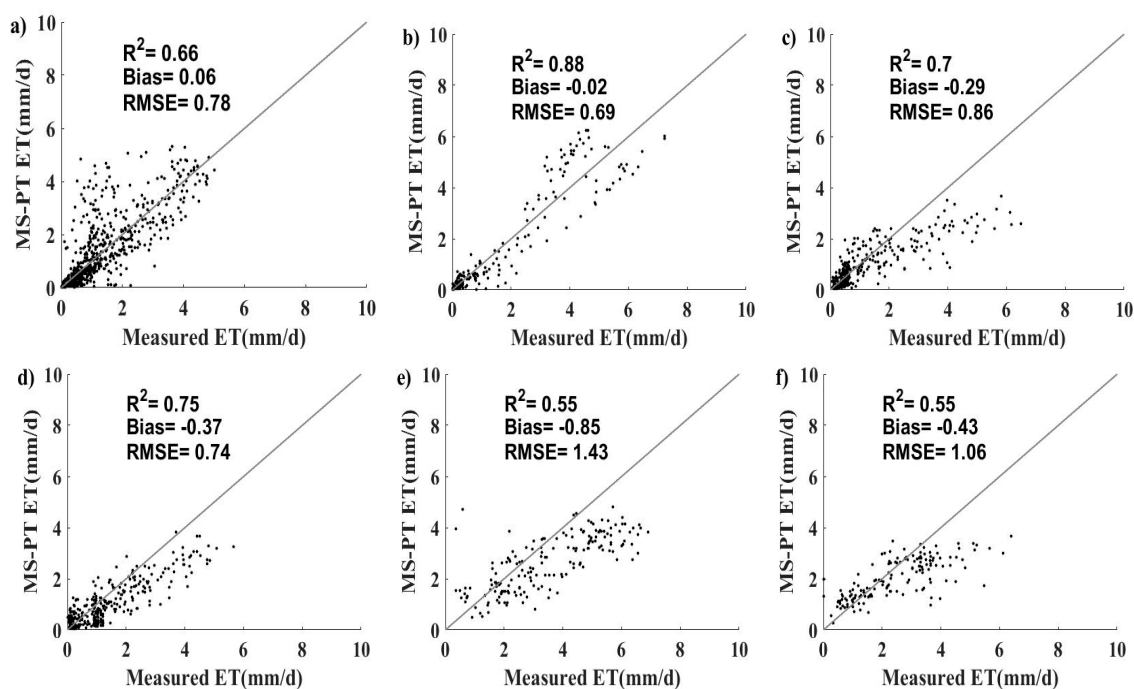
Figure 2. The scatterplots between flux tower observations and estimated ET at daily scale: (**a**) Changbaishan; (**b**) Laoshan; (**c**) Duolun1; (**d**) Duolun2; (**e**) Jinzhou; (**f**) Tongyu. The bias and RMSE are in units of mm/d. The solid line is the 1:1 line.
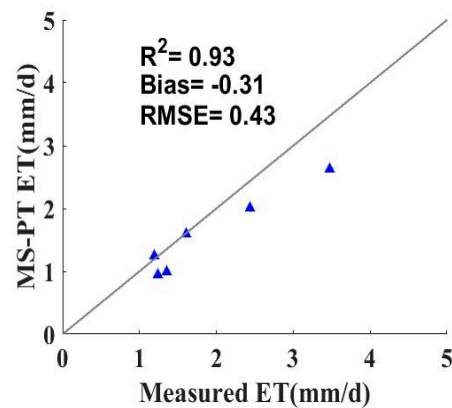
Figure 3. Comparisons of the predicted and measured site-averaged ET at six sites. The bias and RMSE are in units of mm/d. The solid line is the 1:1 line.
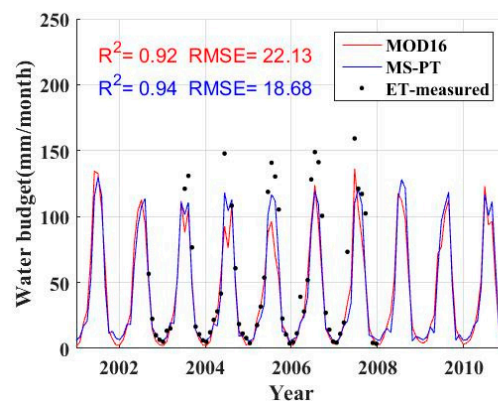

Figure 4. The monthly time series comparison of MS–PT-based ET and MOD16 ET in the Changbaishan station. RMSE is in units of mm/month.

3.2. Mean Spatial Pattern of ET in Northeast China

3.2.1. Annual

The multiyear (1982–2010) average annual ET spatial distribution is shown in Figure 5a. The annual mean ET estimated by the MS–PT algorithm during 1982–2010 is 441.14 ± 18 mm/year in Northeast China. As shown in Figure 5a, the area with lower ET (300–400 mm/year) is mainly distributed in Inner Mongolia, where the land use type is mainly desert and grassland. We also found that the regions with larger ET (500–600 mm/year) were mainly distributed in the eastern part of the LH basin, where croplands and forests were densely distributed. More importantly, this area was also characterized by a relatively abundant precipitation. Moreover, a decreasing trend of ET from the southeast coast to northwest inland is noticeable in Figure 5a. Since Northeast China is located in East Asian monsoon climate zone influenced by the ocean monsoon, the precipitation can directly affect the surface soil moisture, further controlling ET of this region. Thus, compared with the average precipitation and soil moisture pattern (Figure 5b,c), we can clearly find that the annual average ET spatial pattern illustrates the strong regional variation corresponding to the surface water supply.
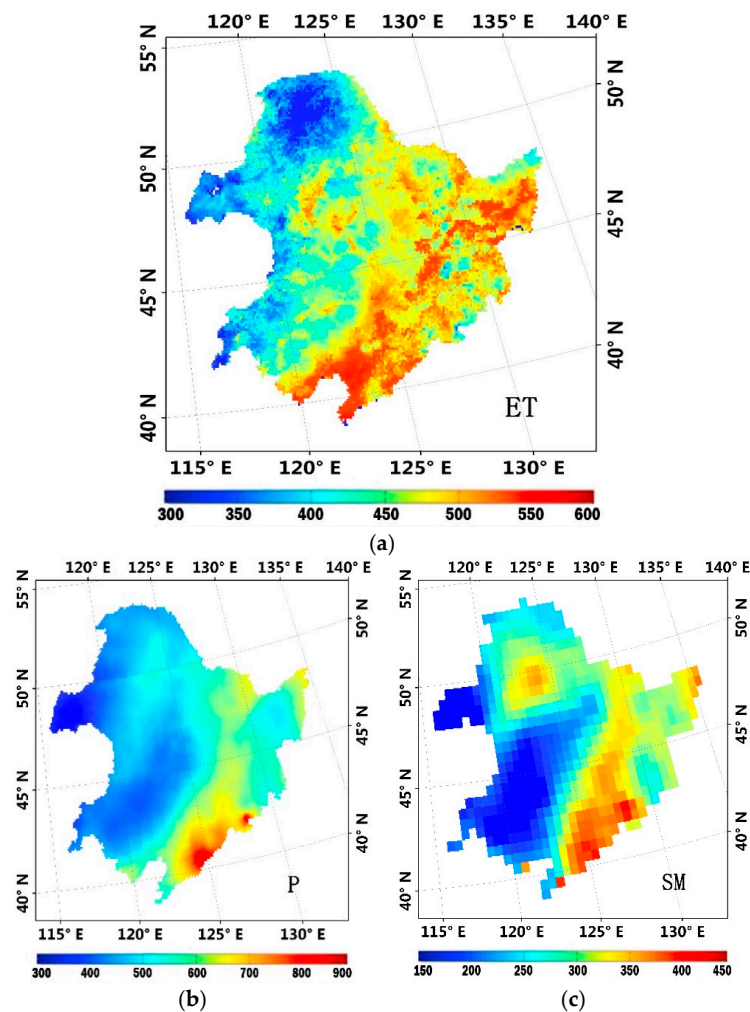
Figure 5. Spatial patterns of (**a**) multiyear average ET, (**b**) multiyear average precipitation, and (**c**) multiyear average soil moisture in Northeast China. All are in units of mm/year.

3.2.2. Seasonal

Multiyear (1982–2010) seasonal patterns of ET over Northeast China are shown in Figure 6. Distinct seasonal cycles of ET can be detected over Northeast China, which corresponds to the East Asian monsoon climate characterized by a wet summer and a dry winter. As shown in Figure 6a, the seasonal mean ET of MAM (March, April, and May) is 20–50 mm/month because of the lower temperature and precipitation. In contrast, during JJA (June, July, and August), when the air temperature and precipitation reach the maximum for the whole year, the monthly ET of most areas in Northeast China exceeds 60 mm/month and accounts for over half of the annual ET (see Figure 6b). After summer, ET has significantly decreased over Northeast China (see Figure 6c,d).

In addition, we also found that the regional distribution characteristic of ET over Northeast China differs among the four seasons. For example, during MAM, peak ET occurs in the southeastern part of the region, which has plentiful solar radiation and rising temperature. However, when summer comes, peak ET expands and moves northward (Figure 6b). Previous study states that, accompanied by plentiful solar radiation, rising air temperature, and fierce vegetation transpiration, the ET of the forest ecosystem is stronger than other ecosystems in the summer [56]. As seen from Figure 6b, the region with high ET is mainly distributed in the north and east regions of Northeast China, where forests were densely distributed. In other words, the distribution of forest determines the distribution characteristic of ET in JJA. When the rainy season has gone and the air temperature is declining, ET has decreased

noticeably from SON (September, October, and November) to DJF (December, January, and February). As a result, the ET of the southern part of the study area is higher than the northern part, which is different from the distribution feature of the ET in JJA.
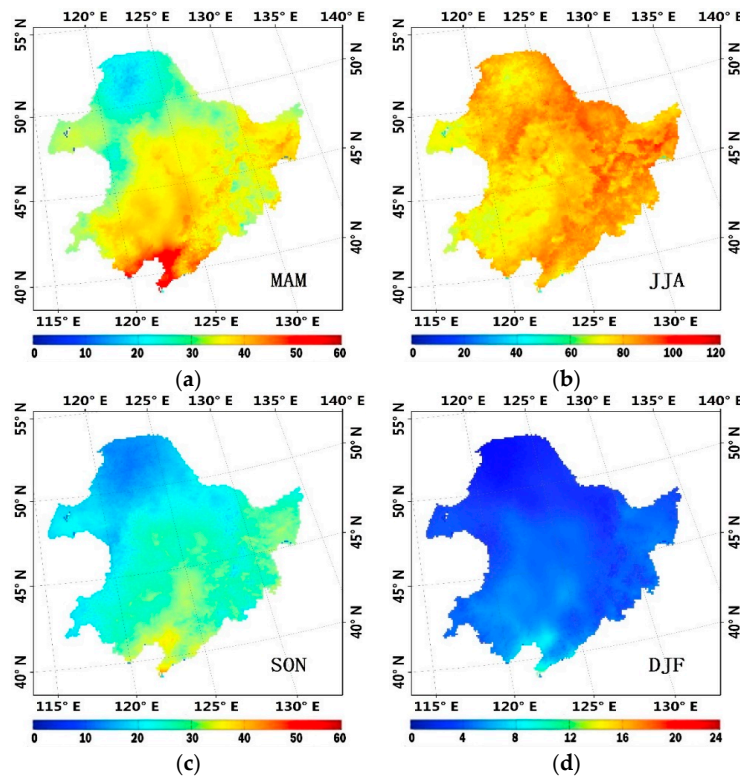

Figure 6. Multiyear seasonal patterns of ET in Northeast China: (**a**) MAM (March, April, and May); (**b**) JJA (June, July, and August); (**c**) SON (September, October, and November); (**d**) DJF (December, January, and February). The ET are in units of mm/month.

3.3. Characteristics of ET Trends

3.3.1. Annual

The ET of Northeast China estimated by MS–PT has increased by 4.5 mm/decade during 1982–2010 (Figure 7a). This increase in annual ET mainly occurred in the period from 1982 to 1998, with a linear trend of 12.3 mm/decade ($p < 0.1$), which is consistent with the expected acceleration in response to global warming [9]. After that, coincident with the last major El Nino event in 1998, the positive trend in ET seems to have ceased, with a non-significant trend of -13.0 mm/decade ($p = 0.42$). The estimates of the trend statistics Z values and the Mann–Kendall slope for annual ET are given in Table 3.

Considering the difference in climatic and hydrological condition between the LH basin and the SJ basin, we further calculated the trend of ET in the SJ basin and the LH basin, respectively. The difference in the ET trends between the pre-1998 period and the post-1998 period became more obvious. As seen from Figure 7b, in the years between 1982 and 1998, the annual land ET of the LH basin increased at a rate of 16.4 mm/decade ($p < 0.01$). After 1998, the annual land ET of the LH basin decreased rapidly with a linear trend of -45.1 mm/decade ($p < 0.01$). This enormous decrease in ET may be driven by the human activity, such as the reclamation of grassland into cropland or the exploitation of mineral resources [20]. Similarly, the annual land ET of the SJ basin increased from 1982 to 1998 with a linear fit having a slope of 11.4 mm/decade. After that, the annual land ET of the SJ basin also decreased by -4.2 mm/decade.
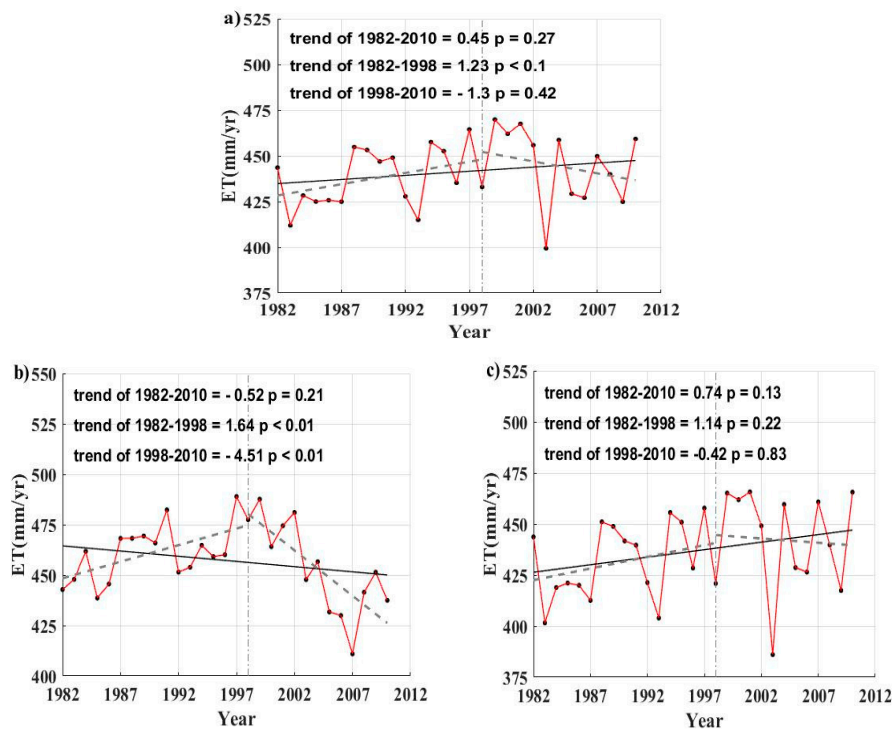
Figure 7. (**a**) Interannual variability of ET from 1982 to 2010 in Northeast China; partly interannual variability of ET: (**b**) the LH basin; and (**c**) the SJ basin.

Table 3. Mann–Kendall test results for the ET trend.

Region	Season	Z	β	R/A
Northeast China	All	1.46	0.45	R
	MAM	−0.14	−0.04	R
	JJA	0.82	0.26	R
	SON	3.24	0.19	A
	DJF	2.42	0.05	A
The LH Basin	All	−0.78	−0.52	R
	MAM	−0.25	−0.13	R
	JJA	−1.57	−0.51	R
	SON	1.07	0.04	R
	DJF	2.71	0.08	A
The SJ Basin	All	2.07	0.74	A
	MAM	0.03	−0.02	R
	JJA	1.74	0.48	R
	SON	3.85	0.24	A
	DJF	2.03	0.04	A

R: reject hypothesis H_0; A: accept hypothesis H_0.

3.3.2. Seasonal

Figure 8 shows interannual land ET variations of Northeast China, the SJ basin, and the LH basin for the four seasons. Except for summer, we found ET increases significantly ($p < 0.1$) from 1982 to 1998 for all periods. However, after 1988, these positive trends appear to have stalled, which is similar to the trend of interannual ET variations. For example, in MAM, ET increased significantly at a rate of 0.4, 0.36, and 0.58 mm·month^{-1} per year from 1982 to 1998 for the whole study area, the SJ basin, and the LH basin, respectively (Figure 8(a–a2)). After 1998, ET decreased year by year, with a rate of −1.05, −0.91, and −1.55 mm·month^{-1} per year for the whole study area, the SJ basin, and the LH basin. The estimates of the trend statistics Z values and the Mann–Kendall slope for seasonal ET are also given in Table 3.
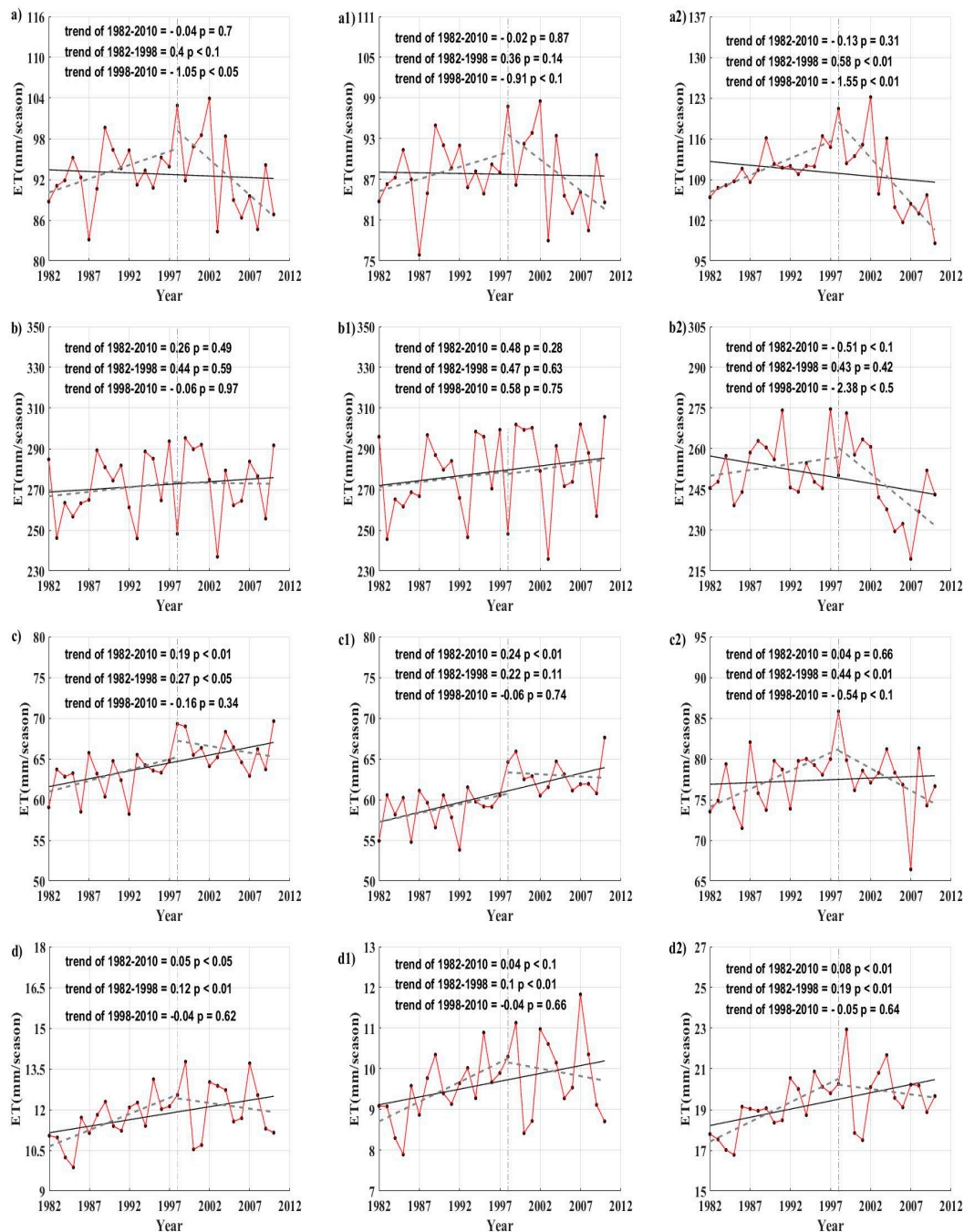
Figure 8. First column: interannual variability of ET from 1982–2010 in Northeast China: (**a**) MAM; (**b**) JJA; (**c**) SON; (**d**) DJF. Second column: interannual variability of ET in the SJ basin: (**a1**) MAM; (**b1**) JJA; (**c1**) SON; (**d1**) DJF. Third column: interannual variability of ET in the LH basin: (**a2**) MAM; (**b2**) JJA; (**c2**) SON; (**d2**) DJF.

We also found the variation trend of interannual land ET has obvious seasonal cycles (Figure 8). The trends of seasonal ET for MAM, SON, and DJF are similar to the annual ET trend. However, for JJA, the annual ET changes irregularly. During 1982–2010, the annual ET of Northeast China increases at a rate of 0.26 mm month^{-1} per year in summer ($p = 0.46$). Such a non-significant increment mainly occurred in the SJ basin with 0.48 mm·month^{-1} per year. For the LH basin, the annual ET decrease at a rate of -0.51 mm·month^{-1} per year in summer ($p < 0.1$). Moreover, the magnitudes of the ET trends changes during JJA are higher than the other three seasons. For example, the annual ET increased at

a rate of 0.47 and 0.43 mm month^{-1} per year in JJA before 1998 over the SJ basin and the LH basin. After 1998, ET still increased 0.58 mm month^{-1} per year in the SJ basin. For the LH basin, the trend of ET becomes negative and significant (-2.38 mm·month^{-1} per year, $p < 0.05$). On the contrary, as seen from Figure 8(d1,d2), the trend of ET is nearly zero for both the SJ basin and the LH basin during 1982–2010 (0.04 mm month^{-1} per year, $p < 0.1$; 0.08 mm·month^{-1} per decade, $p < 0.01$), which is far lower than the trend in JJA. This is because low temperature and limited solar energy restrain soil surface evaporation and vegetation transpiration.

3.4. Spatial Patterns of ET Trend Changes in Northeast China

3.4.1. Annual

Figure 9a shows the spatial distribution of ET trends over Northeast China from 1982 to 2010. Our results illustrate that the ET of Northeast China has increased on average by 6.8 mm/decade during 1982–2010. Fifty-nine percent of the pixels in the study area show an increasing trend in ET and 23.6% of the pixels have a significant increasing trend ($p < 0.05$). Among them, the positive ET trends mainly occur in the north part and east part of the SJ basin, where exactly is vegetated land surface [28]. Only 9.8% of the pixels show a significant decreasing trend and mainly located in the southern part of Inner Mongolia and Western Jilin, which mainly consists of unused land. The reclamation of desert land for cropland has influenced the original ecosystem of these regions and may result in this negative trend of ET [20].
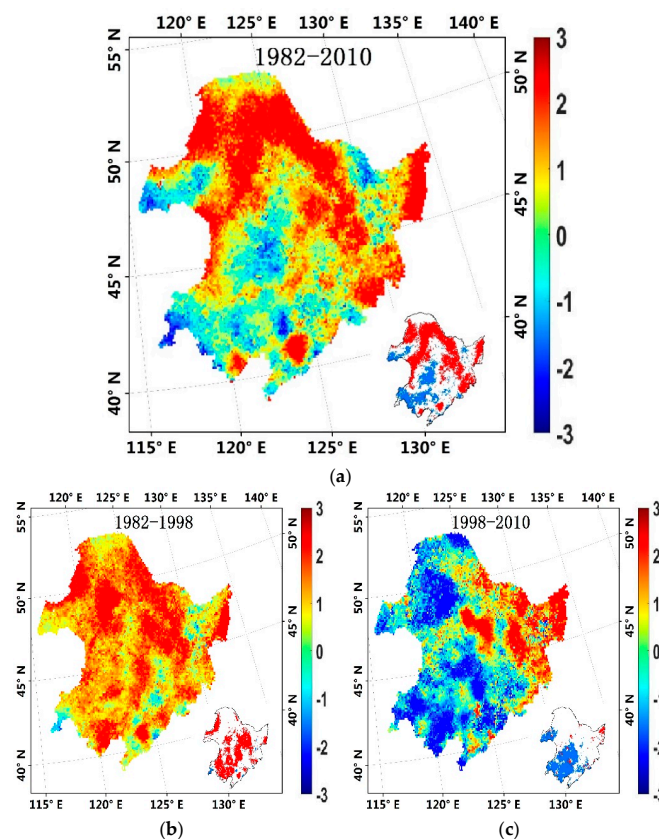
Figure 9. Spatial distributions of ET trends in Northeast China: (**a**) during 1982–2010; (**b**) during 1982–1998; (**c**) during 1998–2010. The ET trend is in units of mm/year. The inset panels show the area where the ET trend is statistically significant ($p < 0.05$). Red represents a significant increase and blue represents a significant decrease.

We also analyzed changes in annual ET trends before and after 1998. We found that, for most regions of Northeast China, the overall increment in annual ET from 1982 to 2010 can largely be attributed to the upward trend of 1982–1998. As shown in Figure 9b, 86.5% of the regions show an upward trend in ET from 1982 to 1998, which is relative to the remarkable warming phenomenon over Northeast China [1]. After 1998, most parts of Northeast China show a negative part, only a few regions of Songjiang basin (32.5%) keep rising in ET (Figure 9c). The difference in ET trends between the two periods indicates that the positive trend of annual ET has ceased, or even reversed.

3.4.2. Seasonal

Figure 10a–d shows the spatial distributions of four seasonal ET trends over Northeast China. From our results, the distribution of interannual land ET trend has obvious seasonal characteristics. In MAM, areas with positive ET trends are mostly located in the LH basin, with its vegetated land surface (Figure 10a). In contrast, for DJF, positive ET trends are mostly located in the SJ basin, with a lower latitude (Figure 10d). As shown in Figure 10b, the spatial distribution of ET trends in JJA is consistent with the annual spatial distribution (Figure 9a), which coincides with the finding by Yang et al. [21]. In summer, ET is the highest among the four seasons. As a result, the ET trend change of JJA can account for most of the total annual ET trend change. We also notice that the spatial distribution of significant trends also coincides with annual significant trends.
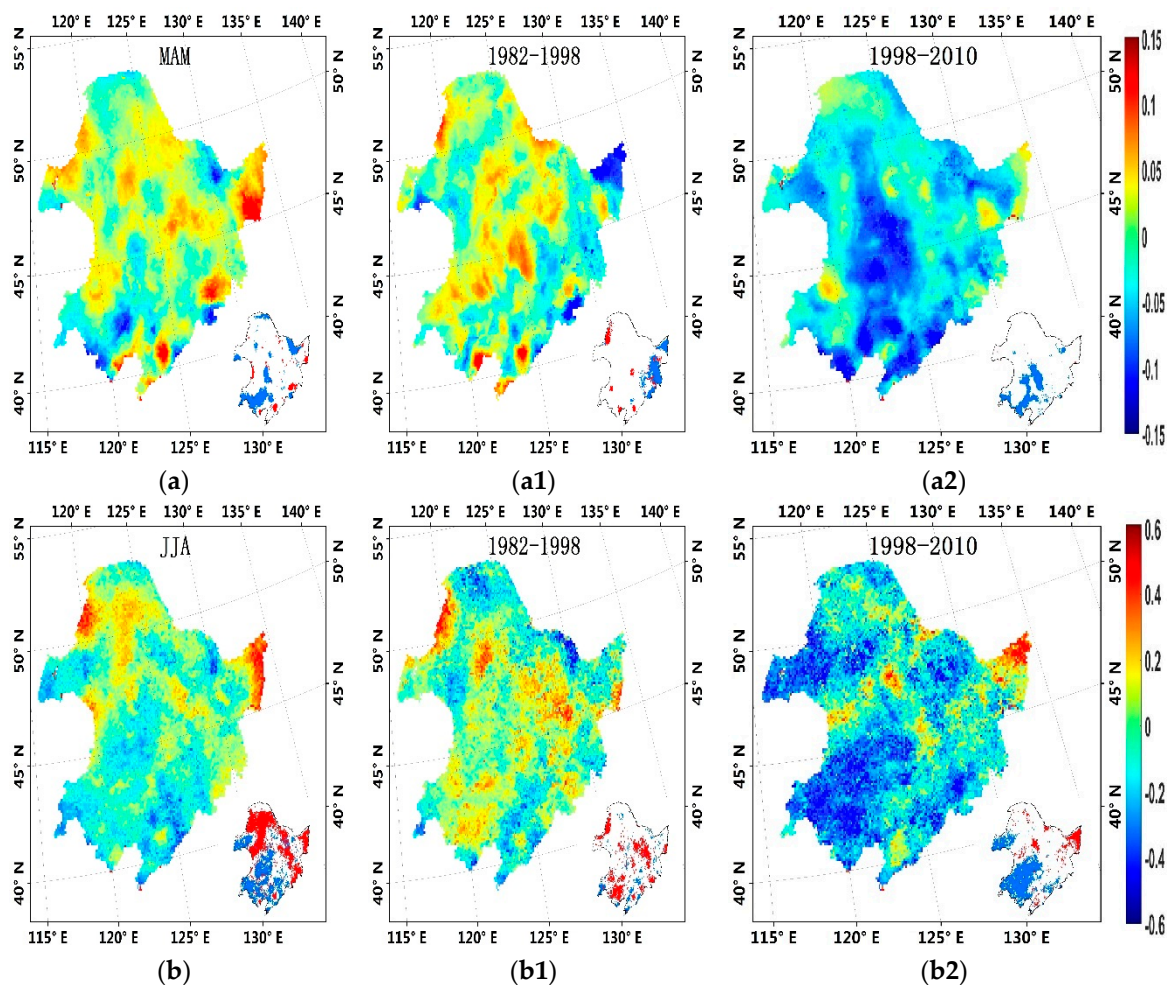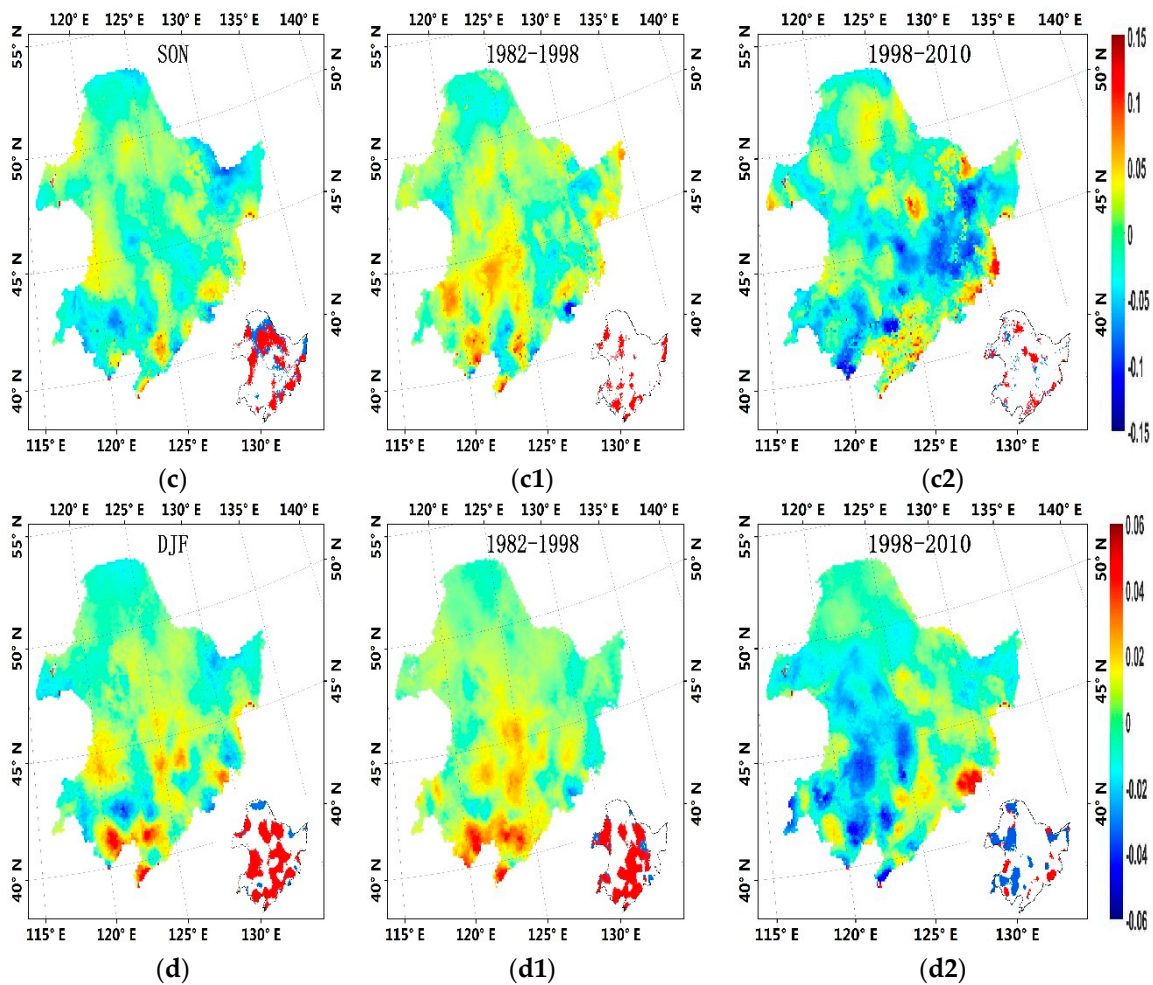

Figure 10. *Cont.*

Figure 10. (First column) Spatial distributions of ET trends in Northeast China during 1982–2010: (**a**) MAM; (**b**) JJA; (**c**) SON; (**d**) DJF; (second column) during 1982–1998: (**a1**) MAM; (**b1**) JJA; (**c1**) SON; (**d1**) DJF; (third column) during 1998–2010: (**a2**) MAM; (**b2**) JJA; (**c2**) SON; (**d2**) DJF. The inset panels show the area where the ET trend is statistically significant ($p < 0.1$).

Then, we analyzed changes in seasonal ET trends before and after 1998. The trend of ET is dominated by that in summer during both the pre-1998 period and the post-1998 period. In other words, the influence of the other three seasons on the trend of annual ET is weaker than JJA. Additionally, the positive annual ET trend change during the four seasons mainly originates from that influence during 1982–1998. Comparing annual ET trends for all seasons before and after 1998, more and more pixels experienced a decreasing trend during the post-1998 period. This is particularly evident for the first half of year, when more pixels of Northeast China show a negative trend change from 1988 to 2010.

4. Discussion

4.1. The Performance of the MS–PT Algorithm in Estimating ET

Model validation at six EC flux tower sites illustrates that the MS–PT algorithm for estimating ET was reliable and robust across multiple biomes in Northeast China (Figure 2). Due to the difference in the water cycle and land surface characteristics, biases exist in the application of global ET products in specific areas [57]. Yao et al. [24] compared the MS–PT algorithm with the PT–JPL algorithm using ground observations collected from 40 flux towers distributed around the world and found MS–PT

algorithm improved ET estimates at most flux towers sites, with a higher R^2 (0.41–0.89) and a lower RMSE (23.7–48.6 W/m^2). Compared with MOD16 product, our results illustrate that the MS–PT algorithm improves the accuracy of ET quantification at most flux tower sites in Northeast China, indicating this method may be a better tool for analyzing the variation of ET over Northeast China. However, one should note that the MS–PT algorithm has a relatively poor performance at flux sites from the CEOP network. Perhaps complex terrain and instrument calibration contribute to large biases.

We also found that the MS–PT algorithm show inter-biome differences and performs better for forest land sites (Figure 2). The seasonality for vegetation indices and canopy structure may be critical in determining satellite-based ET model performance [58]. Previous studies have revealed that some satellite-based ET algorithms can estimate ET more accurately for deciduous broadleaf forest [46,59]. Since the major seasonal vegetation types of the forest region in Northeast China are deciduous broadleaf forest and coniferous forest [25,60], our validation results are similar with previous findings. In contrast, for some cropland and grassland sites, such as the Jinzhou flux site, the MS–PT algorithm still has relatively low R^2 and high RMSE. The limitation of the MS–PT algorithm, such as neglecting of the differences in parameters from different biome types, may cause this problem [24].

We should note that the accuracy of MS–PT algorithm depends on the errors for EC ET observations because we consider ET observations as true values in calculating the weights for the MS–PT algorithm. Although we correct ET by Twine et al. [43] method, the inaccuracy in the measured data still exists, such as the energy imbalance issue, with H + LE < $R_n - G$ (H: sensible heat flux; LE: latent heat flux) [61]. The mismatches in scale among different datasets may also lead to differences between the simulated and measured values. For example, the original spatial resolutions of meteorological reanalysis data and the NDVI3g data are 0.1 degree and 8 km, respectively. While the NDVI3g data was converted to a resolution of $0.1° \times 0.1°$ using bilinear interpolation, the resample process may also result in biases. Additionally, EC observations represent a point-based value with merely hundreds of meters in diameter, which may also cause differences between ET observations and the true ET [62]. If the input data has a higher spatial resolution, the performance of MS–PT can be greatly improved.

4.2. Climate Change Controls on Land ET Trends in Northeast China

Major global climatic perturbations and influences, such as the last major El Niño event in 1998, have caused alterations in the global water cycle and land–atmosphere water flux [46]. Our findings confirm that ET of Northeast China has increased significantly ($p < 0.1$) over the last two decades of the twentieth century [19] and decreased with large interannual fluctuations ($p = 0.42$) after 1998 (Figure 6a) [20]. Most previous studies suggest that the limitation by surface water supply is the dominant factor in determining this ET trend change [7,22,63,64], because of the relatively sparse precipitation in some regions of Northern China. However, some studies propose that the changes in the ET trend may be the result of the variation in air temperature, vegetation condition, or surface energy [56,65–68]. Additionally, due to the nonlinear dependence of ET on related climate factors, their relative contributions to the ET trend are not obvious. Thus, it is difficult to assess climate change controls on ET trends in Northeast China.

In this study, based on the interannual variations of ET calculated by MS–PT algorithm, we find moderate spatial correlation between the trend of ET and precipitation in the west part of Northeast China (Figure 11a). Only in the western region of Northeast China, where annual rainfall is infrequent, the trend of precipitation shows a positive correlation with the variation of ET. Similarly, the trend of soil moisture also shows a correlation with ET trends in this area (Figure 11b). These positive correlations can be explained by the fact that, under dry condition (Figure 5b), less precipitation leads to lower soil moisture, which, in turn, limits ET [69]. Furthermore, a reduced ET would decrease the precipitation and further reduce soil moisture [70,71]. Therefore, precipitation can play a key role for the annual variation of ET. However, in other areas of Northeast China, weak spatial consistency is found between ET trend changes and precipitation trend changes, which is also documented by

Tian et al. [19]. It is possible that different surface vegetation and water supply cause the consistency difference. For instance, there is more deep-rooted vegetation in the northern part of Northeast China, where roots of the vegetation can reach groundwater and extract water from the whole layer of soil [72]. As a result, precipitation is no longer a good indication of ET in these areas, which is different from previous studies. In a word, only under dry conditions, such as the western region of Northeast China, is precipitation is a critical meteorological factor influencing ET trend.
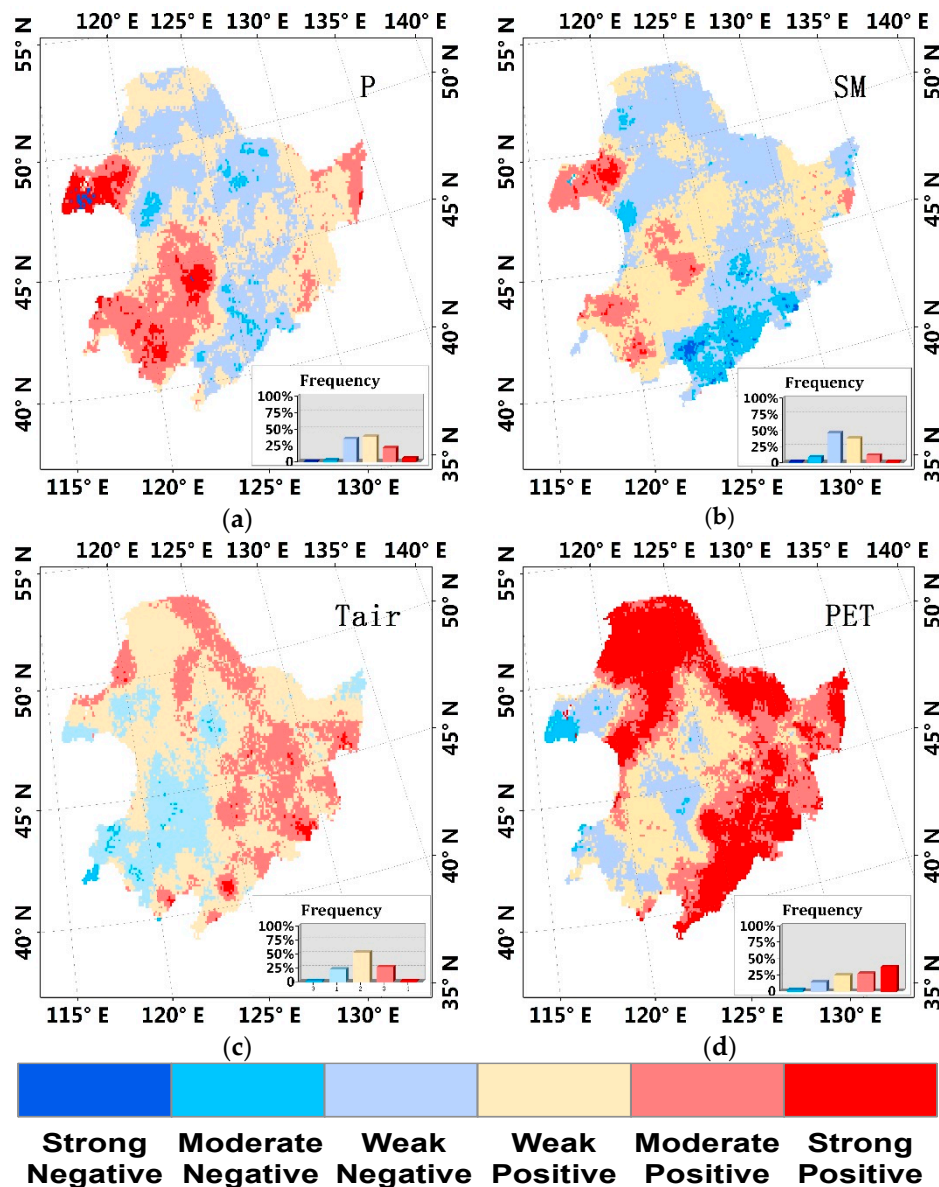
Figure 11. Map of the correlation coefficient between the annual ET trend (1982–2010) and the trend of (**a**) precipitation, (**b**) soil moisture, (**c**) Tair, and (**d**) PET. The inset panels show the frequency of various change trends. The degree of correlation is classified into three ranks according to the correlation coefficient: strong ($R^2 \geq 0.7$); moderate ($0.3 < R^2 < 0.7$); weak ($R^2 \leq 0.3$).

As shown in Figure 5c, in the humid areas, such as the southeast coast and north part of Northeast China, the changes in ET are unrestricted by water supply because of relatively abundant soil moisture. PET, an important indicator of atmospheric evaporation demand, represents the maximum ET rate when given an unlimited water supply and may influence the trends of ET in these areas [73,74]. Mo et al. [56] suggested that there exists an opposite trend of ET and PET in China, which reveals

a complementary relationship between ET and PET. Gao et al. [7] found that the decreasing PET largely influences the decreasing trends of ET in Southeast China and proposed that the change of PET appeared to be the major factor determining the change of actual ET in subtropical humid area. However, we found a strong spatial correlation between PET trend changes and ET trend changes in wet regions of Northeast China, which demonstrates that PET may be the dominant factor determining the trend changes in ET (Figure 11d). Moreover, previous substantial studies suggest that Tair is a key controlling factor influencing ET in high latitude region [75], because it can be recognized as a surrogate for atmospheric demand [76]. Our results illustrate that the trend of Tair is positively related to ET trends in these areas (Figure 11c), but the correlation is weaker than PET. This can be explained that PET is influenced by a number of climate elements, including Tair, net radiation, wind speed, and vapor pressure, and ET is limited by freezing temperatures, wind speed, and surface energy in Northeast China [77]. Integrated with different climatic factors, PET appears to better control the trend of ET. Overall, in high latitude and wet canopy conditions, PET tends to exert the most significant control over ET.

5. Conclusions

The goal of this study was to estimate terrestrial ET of Northeast China during 1982–2010 using the MS–PT algorithm. This approach in modeling ET is physically based, requiring no subjective parameter calibration as employed by many other traditional ET methods. Using the ET measurements of the six eddy covariance sites, our validation showed MS–PT algorithm provided the reliable ET estimations at site scale. We also used meteorological reanalysis data and remote sensing data to analyze the spatiotemporal variation in ET during 1982–2010. The results demonstrated that MS–PT algorithm has a good performance in estimating regional ET over Northeast China.

In this paper, we found the annual mean ET during 1982–2010 is 440.68 ± 18 mm/year in Northeast China. For the spatial pattern of annual averaged ET over Northeast China, we found a decreasing trend from southeast coast to northwest inland, which is influenced by the surface water resource. Over the entire study area, ET has increased on average by 5 mm year^{-1} per decade over Northeast China during 1982–2010, and the pixels with a positive trend were mainly distributed in the SJ basin. We found an especially obvious difference before and after 1998 and concluded that the increase in annual ET mainly occurred in the period from 1982 to 1998. Further, we evaluate what have caused any spatial-temporal variation in ET. Our findings illustrate that PET is the most important factor influencing ET trend in most parts of Northeast China. Over semiarid and arid areas, such as the west of Northeast China, precipitation can also affect ET variation. Thus, future studies are needed to clarify the relative contributions of the different climatic variables and understand the contributing process of different climatic variables in ET.

Author Contributions: Lilin Zhang, Yunjun Yao, and Zhiqiang Wang prepared the manuscript. Xuanyu Wang, Jia Xu, and Xiaowei Chen conducted the remote sensing image processing. Kun Jia, Xiaotong Zhang, and Yuhu Zhang contributed to the discussion.

References

1. Sun, F.H.; Yang, X.Q.; Lu, S.; Yang, S.Y. The contrast analysis on the average and extreme temperature trend in northeast china. *Sci. Meteorol. Sin.* **2006**, *26*, 157–163.
2. Mao, D.; Wang, Z.; Luo, L.; Yang, G. Correlation analysis between ndvi and climate in northeast china based on avhrr and gimms data sources. *Remote Sens. Technol. Appl.* **2012**, *27*, 81–89.
3. Wang, K.; Dickinson, R.E. A review of global terrestrial evapotranspiration: Observation, modeling, climatology, and climatic variability. *Rev. Geophys.* **2012**, *50*. [CrossRef]
4. Yao, Y.; Liang, S.; Li, X.; Chen, J.; Wang, K.; Jia, K.; Cheng, J.; Jiang, B.; Fisher, J.B.; Mu, Q. A satellite-based hybrid algorithm to determine the priestley-taylor parameter for global terrestrial latent heat flux estimation across multiple biomes. *Remote Sens. Environ.* **2015**, *165*, 216–233. [CrossRef]
5. Yao, Y.; Liang, S.; Yu, J.; Chen, J.; Liu, S.; Lin, Y.; Fisher, J.B.; Mcvicar, T.R.; Cheng, J.; Jia, K. A simple temperature domain two-source model for estimating agricultural field surface energy fluxes from Landsat images. *J. Geophys. Res. Atmos.* **2017**. [CrossRef]
6. Sun, F.; Wu, Z.; Yang, S. Temporal and spatial variations of extreme precipitation and dryness events in northeast china in last 50 years. *Chin. J. Ecol.* **2006**, *25*, 779–784.
7. Gao, G.; Chen, D.; Xu, C.Y.; Simelton, E. Trend of estimated actual evapotranspiration over china during 1960–2002. *J. Geophys. Res. Atmos.* **2007**, *112*, 71–81. [CrossRef]
8. Zhang, S.J.; Zhang, Y.S.; Sui, D.; Cai, F.; Fu, C.; Wu, J.-W.; Chen, P.S.; Liu, Q.W. Changes in reference evapotranspiration and its causes in northeast china. *J. Nat. Resour.* **2010**, *25*, 1750–1761.
9. Jung, M.; Reichstein, M.; Ciais, P.; Seneviratne, S.I.; Sheffield, J.; Goulden, M.L.; Bonan, G.; Cescatti, A.; Chen, J.; De, J.R. Recent decline in the global land evapotranspiration trend due to limited moisture supply. *Nature* **2010**, *467*, 951–954. [CrossRef] [PubMed]
10. Wang, K.; Dickinson, R.E.; Wild, M.; Liang, S. Evidence for decadal variation in global terrestrial evapotranspiration between 1982 and 2002. *J. Geophys. Res. Atmos.* **2010**, *115*, 898–907. [CrossRef]
11. Shukla, J.; Mintz, Y. Influence of land-surface evapotranspiration on the earth's climate. *Science* **1982**, *215*, 1498–1501. [CrossRef] [PubMed]
12. Zeng, L.H.; Song, K.S.; Zhang, B.; Wang, Z.M.; Du, J. Spatiotemporal variability of reference evapotranspiration over the northeast region of china in the last 60 years. *Adv. Water Sci.* **2010**, *21*, 194–200.
13. Zhang, B.; Kang, S.; Li, F.; Zhang, L. Comparison of three evapotranspiration models to bowen ratio-energy balance method for a vineyard in an arid desert region of northwest china. *Agric. For. Meteorol.* **2008**, *148*, 1629–1640. [CrossRef]
14. Liu, S.M.; Xu, Z.W.; Wang, W.Z.; Jia, Z.Z.; Zhu, M.J.; Bai, J.; Wang, J.M. A comparison of eddy-covariance and large aperture scintillometer measurements with respect to the energy balance closure problem. *Hydrol. Earth Syst. Sci.* **2011**, *15*, 1291–1306. [CrossRef]
15. Allen, R.G.; Pereira, L.S.; Raes, D.; Smith, M. Crop Evapotranspiration-Guidelines for Computing Crop Water Requirements. Available online: https://appgeodb.nancy.inra.fr/biljou/pdf/Allen_FAO1998.pdf (accessed on 1 November 2017).
16. Yang, Y. Remote sensing temporal and spatial patterns of evapotranspiration and the responses to water management in a large irrigation district of north china. *Agric. For. Meteorol.* **2012**, *164*, 112–122. [CrossRef]
17. Zhang, K.; Kimball, J.S.; Nemani, R.R.; Running, S.W. A continuous satellite-derived global record of land surface evapotranspiration from 1983 to 2006. *Water Resour. Res.* **2010**, *46*, 109–118. [CrossRef]
18. Mueller, B.; Hirschi, M.; Jimenez, C.; Ciais, P. Benchmark products for land evapotranspiration: Landflux-eval multi-dataset synthesis. *Hydrol. Earth Syst. Sci.* **2013**, *17*, 3707–3720. [CrossRef]
19. Tian, J.; Hongbo, S.U.; Chen, S.; Sun, X.; Chen, Q. Spatial-temporal variations of evapotranspiration in china mainland in recent 20 years. *Resour. Sci.* **2012**, *34*, 1277–1286.
20. Tian, H.E.; Shao, Q. Spatial-temporal variation of terrestrial evapotranspiration in china from 2001 to 2010 using mod16 products. *J. Geo-Inf. Sci.* **2014**, *16*, 979–988.
21. Yang, X.; Wang, G.; Pan, X.; Zhang, Y. Spatio-temporal variability of terrestrial evapotranspiration in china from 1980 to 2011 based on gleam data. *Trans. Chin. Soc. Agric. Eng.* **2015**, *31*, 132–141.
22. Chen, Y.; Xia, J.; Liang, S.; Feng, J.; Fisher, J.B.; Li, X.; Li, X.; Liu, S.; Ma, Z.; Miyata, A. Comparison of satellite-based evapotranspiration models over terrestrial ecosystems in china. *Remote Sens. Environ.* **2014**, *140*, 279–293. [CrossRef]

23. Yao, Y.; Liang, S.; Cheng, J.; Liu, S.; Fisher, J.B.; Zhang, X.; Jia, K.; Zhao, X.; Qin, Q.; Zhao, B. Modis-driven estimation of terrestrial latent heat flux in china based on a modified priestley-taylor algorithm. *Agric. For. Meteorol.* **2013**, *171–172*, 187–202. [CrossRef]

24. Yao, Y.; Liang, S.; Zhao, S.; Zhang, Y.; Qin, Q.; Cheng, J.; Jia, K.; Xie, X.; Zhang, N.; Liu, M. Validation and application of the modified satellite-based priestley-taylor algorithm for mapping? Terrestrial evapotranspiration. *Remote Sens.* **2014**, *6*, 880–904. [CrossRef]

25. Mao, D.H.; Wang, Z.M.; Han, J.X.; Ren, C.Y. Spatio-temporal Pattern of Net Primary Productivity and Its Driven Factors in Northeast China in 1982–2010. *Sci. Geogr. Sin.* **2012**. [CrossRef]

26. Tang, Y.; Wang, H.; Yan, D.H.; Wang, S.S. Research on the spatial-temporal differentiation of precipitation in northeast China in recent 50 years. *Sci. Geogr. Sin.* **2005**, *18*, 901–906.

27. Qian, Z. Strategic concern to land and water resources allocation, ecology and environment protection and sustainable development of northeast China. *Eng. Sci.* **2006**, *8*, 1–24.

28. Liu, J.Y.; Kuang, W.H.; Zhang, Z.X.; Xu, X.L.; Qin, Y.W.; Ning, J.; Zhou, W.C.; Zhang, S.W.; Li, R.D.; Yan, C.Z.; et al. Spatiotemporal characteristics, patterns, and causes of land-use changes in China since the late 1980s. *J. Geogr. Sci.* **2014**, *24*, 195–210. [CrossRef]

29. Wang, X.Q.; Zhang, Y.; Liu, C.M. Estimation of eco-water requirement in the liaohe river basin. *Geogr. Res.* **2007**, *26*, 22–28.

30. Han, J.X.; Wang, Z.M.; Mao, D.H.; Song, K.S.; Ren, C.Y. Dynamic change of vegetation coverage in the songhua river basin and itscorrelation analysis with climatic factor from 1982 to 2010. *Chin. J. Agrometeorol.* **2011**, *32*, 430–436.

31. Liu, Q. A study on flood and drought change and its long-term prediction in the songhua river basin. *Adv. Water Sci.* **1994**, *4*, 319–327.

32. National Oceanic and Atmospheric Administration, Avhrr. Available online: http://islscp2.sesda.com/ISLSCP21/data (accessed on 24 November 2016).

33. National Aeronautics and Space Administration, lp Daac. Available online: http://reverb.echo.nasa.gov/reverb (accessed on 16 October 2016).

34. Mu, Q.; Heinsch, F.A.; Zhao, M.; Running, S.W. Development of a global evapotranspiration algorithm based on modis and global meteorology data. *Remote Sens. Environ.* **2007**, *111*, 519–536. [CrossRef]

35. Mu, Q.; Zhao, M.; Running, S.W. Improvements to a modis global terrestrial evapotranspiration algorithm. *Remote Sens. Environ.* **2011**, *115*, 1781–1800. [CrossRef]

36. National Oceanic and Atmospheric Administration/oar/esrl psd, Boulder, Colorado, USA. Available online: http://www.esrl.noaa.gov/psd/ (accessed on 19 September 2016).

37. He, J.; Yang, K. China meteorological forcing dataset. In *Cold and Arid Regions Science Data Center at Lanzhou*. Available online: http://westdc.westgis.ac.cn/ (accessed on 26 December 2016).

38. Yang, K.; Jie, H.; Tang, W.; Qin, J.; Cheng, C.C.K. On downward shortwave and longwave radiations over high altitude regions: Observation and modeling in the tibetan plateau. *Agric. For. Meteorol.* **2010**, *150*, 38–46. [CrossRef]

39. Chen, Y.; Yang, K.; Jie, H.; Qin, J.; Shi, J.; Du, J.; He, Q. Improving land surface temperature modeling for dry land of china. *J. Geophys. Res. Atmos.* **2011**, *116*, D20104. [CrossRef]

40. Guirui, Y.U.; Zhang, L.; Sun, X. Progresses and prospects of chinese terrestrial ecosystem flux observation and research network (chinaflux). *Prog. Geogr.* **2014**, *33*, 903–917.

41. Jia, Z.; Liu, S.; Xu, Z.; Chen, Y.; Zhu, M. Validation of remotely sensed evapotranspiration over the hai river basin, china. *J. Geophys. Res. Atmos.* **2012**, *117*, 13113. [CrossRef]

42. Yao, Y.; Liang, S.; Li, X.; Liu, S.; Chen, J.; Zhang, X.; Jia, K.; Jiang, B.; Xie, X.; Munier, S. Assessment and simulation of global terrestrial latent heat flux by synthesis of cmip5 climate models and surface eddy covariance observations. *Agric. For. Meteorol.* **2016**, *223*, 151–167. [CrossRef]

43. Twine, T.E.; Kustas, W.P.; Norman, J.M.; Cook, D.R.; Houser, P.R.; Teyers, T.P.; Prueger, J.H.; Starks, P.J.; Wesely, M.L. Correcting eddy-covariance flux underestimates over a grassland. *Agric. For. Meteorol.* **2000**, *103*, 279–300. [CrossRef]

44. Monteith, J.L. Evaporation and environment. *Symp. Soc. Exp. Biol.* **1965**, *19*, 205. [PubMed]

45. Priestley, C.H.B.; Taylor, R.J. On the assessment of surface heat flux and evaporation using large-scale parameters. *Mon. Weather Rev.* **2009**, *100*, 81–92. [CrossRef]

46. Fisher, J.B.; Tu, K.P.; Baldocchi, D.D. Global estimates of the land-atmosphere water flux based on monthly avhrr and islscp-ii data, validated at 16 fluxnet sites. *Remote Sens. Environ.* **2008**, *112*, 901–919. [CrossRef]

47. Wang, K.; Liang, S. Estimation of surface net radiation from solar shortwave radiation measurements. In Proceedings of the IEEE International Geoscience and Remote Sensing, Boston, MA, USA, 7–11 July 2008; pp. 483–486.

48. Chen, S.; Liu, Y.; Thomas, A. Climatic change on the tibetan plateau: Potential evapotranspiration trends from 1961–2000. *Clim. Chang.* **2006**, *76*, 291–319.

49. Yao, Y.; Zhao, S.; Zhang, Y.; Jia, K.; Liu, M. Spatial and decadal variations in potential evapotranspiration of china based on reanalysis datasets during 1982–2010. *Atmosphere* **2014**, *5*, 737–754. [CrossRef]

50. Mann, H.B. Nonparametric test against trend. *Econometrica* **1945**, *13*, 245–259. [CrossRef]

51. Kendall, M.G. *Rank Correlation Methods*; University of Michigan: Ann Arbor, MI, USA, 1948.

52. Rahman, A.; Dawood, M. Spatio-statistical analysis of temperature fluctuation using Mann-Kendall and Sen's slope approach. *Clim. Dyn.* **2017**, *48*, 1–15.

53. Batra, N.; Islam, S.; Venturini, V.; Bisht, G.; Jiang, L. Estimation and comparison of evapotranspiration from modis and avhrr sensors for clear sky days over the southern great plains. *Remote Sens. Environ.* **2006**, *103*, 1–15. [CrossRef]

54. Seguin, B.; Becker, F.; Phulpin, T.; Gu, X.F.; Guyot, G.; Kerr, Y.; King, C.; Lagouarde, J.P.; Ottlé, C.; Stoll, M.P. Irsute: A minisatellite project for land surface heat flux estimation from field to regional scale. *Remote Sens. Environ.* **1999**, *68*, 357–369. [CrossRef]

55. Kalma, J.D.; Mcvicar, T.R.; Mccabe, M.F. Estimating land surface evaporation: A review of methods using remotely sensed surface temperature data. *Surv. Geophys.* **2008**, *29*, 421–469. [CrossRef]

56. Lin, Z. Trends in land surface evapotranspiration across china with remotely sensed ndvi and climatological data for 1981–2010. *Hydrol. Sci. J.* **2015**, *60*, 2163–2177.

57. Li, Z.L.; Tang, R.; Wan, Z.; Bi, Y.; Zhou, C.; Tang, B.; Yan, G.; Zhang, X. A review of current methodologies for regional evapotranspiration estimation from remotely sensed data. *Sensors* **2009**, *9*, 3801. [CrossRef] [PubMed]

58. Yebra, M.; Dijk, A.V.; Leuning, R.; Huete, A.; Guerschman, J.P. Evaluation of optical remote sensing to estimate actual evapotranspiration and canopy conductance. *Remote Sens. Environ.* **2013**, *129*, 250–261. [CrossRef]

59. Vinukollu, R.K.; Meynadier, R.; Sheffield, J.; Wood, E.F. Multi-model, multi-sensor estimates of global evapotranspiration: Climatology, uncertainties and trends. *Hydrol. Process.* **2011**, *25*, 3993–4010. [CrossRef]

60. Wang, Z.M.; Guo, Z.X.; Song, K.S.; Ling, L.; Bai, Z.; Liu, D.W.; Ni, H.; Ren, C.Y. Responses of vegetation ndvi in northeast china to climate change. *Chin. J. Ecol.* **2009**, *28*, 1041–1048.

61. Yao, Y.; Liang, S.; Li, X.; Hong, Y.; Fisher, J.B.; Zhang, N.; Chen, J.; Cheng, J.; Zhao, S.; Zhang, X. Bayesian multimodel estimation of global terrestrial latent heat flux from eddy covariance, meteorological, and satellite observations. *J. Geophys. Res. Atmos.* **2014**, *119*, 4521–4545. [CrossRef]

62. Liang, S.; Wang, K.; Zhang, X.; Wild, M. Review on estimation of land surface radiation and energy budgets from ground measurement, remote sensing and model simulations. *IEEE J. Sel. Top. Appl. Earth Obs. Remote Sens.* **2010**, *3*, 225–240. [CrossRef]

63. Zhou, L.; Wang, S.; Cheng, J.; Feng, X.; Ju, W.; Wu, W. The spatial-temporal characteristics of evapotranspiration of China's terrestrial ecosystems during 1991–2000. *Resour. Sci.* **2009**, *31*. [CrossRef]

64. Mcvicar, T.R.; Roderick, M.L.; Donohue, R.J.; Li, L.T.; Niel, T.G.V.; Thomas, A.; Grieser, J.; Jhajharia, D.; Himri, Y.; Mahowald, N.M. Global review and synthesis of trends in observed terrestrial near-surface wind speeds: Implications for evaporation. *J. Hydrol.* **2012**, *416–417*, 182–205. [CrossRef]

65. Liu, M.; Tian, H.; Chen, G.; Ren, W.; Zhang, C.; Liu, J. Effects of land-use and land-cover change on evapotranspiration and water yield in China during 1900-2000. *JAWRA J. Am. Water Resour. Assoc.* **2008**, *44*, 1193–1207. [CrossRef]

66. Zhou, L.; Zhou, G. Measurement and modelling of evapotranspiration over a reed (phragmites australis) marsh in northeast China. *J. Hydrol.* **2009**, *372*, 41–47. [CrossRef]

67. Han, Z.; Guirui, Y.U.; Wang, Q.; Zhu, X.; Honglin, H.E.; Wang, Y.; Zhang, J.; Yingnian, L.I.; Liang, Z.; Zhao, F. Spatial variation in annual actual evapotranspiration of terrestrial ecosystems in china: Results from eddy covariance measurements. *J. Geogr. Sci.* **2016**, *26*, 1391–1411.

68. Penman, H.L. Natural evaporation from open water, hare soil and grass. *Proc. R. Soc. Lond. A Math. Phys.* **1948**, *193*, 120. [CrossRef]

69. Zeng, Z.; Wang, T.; Zhou, F.; Ciais, P.; Mao, J.; Shi, X.; Piao, S. A worldwide analysis of spatiotemporal changes in water balance-based evapotranspiration from 1982 to 2009. *J. Geophys. Res. Atmos.* **2014**, *119*, 1186–1202. [CrossRef]

70. Koster, R.D.; Suarez, M.J. A simple framework for examining the interannual variability of land surface moisture fluxes. *J. Clim.* **1999**, *12*, 1911–1917. [CrossRef]

71. Koster, R.D.; Dirmeyer, P.A.; Guo, Z.; Bonan, G.; Chan, E.; Cox, P.; Gordon, C.T.; Kanae, S.; Kowalczyk, E.; Lawrence, D. Regions of strong coupling between soil moisture and precipitation. *Science* **2004**, *305*, 1138. [CrossRef] [PubMed]

72. Federer, C.A.; Vörösmarty, C.; Fekete, B. Sensitivity of annual evaporation to soil and root properties in two models of contrasting complexity. *J. Hydrometeorol.* **2003**, *4*, 1276–1290. [CrossRef]

73. Thomas, A. Spatial and temporal characteristics of potential evapotranspiration trends over China. *Int. J. Climatol.* **2015**, *20*, 381–396. [CrossRef]

74. Zhao, S.H.; Yang, Y.H.; Zhang, F.; Sui, X.X.; Yao, Y.J.; Zhao, N.; Zhao, Q.; Li, C.Q. Rapid evaluation of reference evapotranspiration in northern China. *Arab. J. Geosci.* **2015**, *8*, 647–657. [CrossRef]

75. Iwasaki, H.; Saito, H.; Kuwao, K.; Maximov, T.C.; Hasegawa, S. Forest decline caused by high soil water conditions in a permafrost region. *Hydrol. Earth Syst. Sci. Discuss.* **2010**, *14*, 301–307. [CrossRef]

76. Wang, K.; Dickinson, R.E.; Liang, S. Global atmospheric evaporative demand over land from 1973 to 2008. *J. Clim.* **2012**, *25*, 8353–8361. [CrossRef]

77. Gao, G.; Chen, D.; Ren, G.; Chen, Y.; Liao, Y. Spatial and temporal variations and controlling factors of potential et in China: 1956–2000. *J. Geogr. Sci.* **2006**, *16*, 3–12. [CrossRef]